In Situ Infrared Spectroscopy of Catalytic Solid−Liquid Interfaces Using Phase-Sensitive Detection: Enantioselective Hydrogenation of a Pyrone over Pd/TiO_2

Thomas Bürgi* and Alfons Baiker

Laboratory of Technical Chemistry, Swiss Federal Institute of Technology, ETH Hönggerberg, CH-8093 Zürich, Switzerland

Received: February 4, 2002; In Final Form: July 1, 2002

The potential of modulation excitation spectroscopy and phase-sensitive detection in combination with attenuated total reflection (ATR) for in situ infrared spectroscopy of catalytic solid−liquid interfaces is demonstrated. The method is based on the periodic variation of an external parameter such as reactant concentration. The periodically varying signals are subsequently demodulated using a phase-sensitive detection scheme. In this way, the small periodically varying signals are separated from the large static ones, yielding high quality difference spectra. Species, which have different response to the excitation, i.e., species with different kinetics, can easily be separated in the spectra. The method is applied to the enantioselective hydrogenation of 4-methoxy-6-methyl-2-pyrone over a 5 wt % Pd/TiO_2 powder catalyst modified by cinchonidine. Upon modulation of the reactant concentration, the ATR spectra exhibit varying signals from dissolved reactant, product as well as from adsorbed species. Part of the signals are associated with carboxylates adsorbed on the TiO_2. The kinetics of these species are distinctly different from the one of the primary hydrogenation product. The carboxylates are formed from alcoholysis of the lactone, which is obtained by a second hydrogenation step. The enantiomeric excess was also measured phase sensitive. Its time dependence indicates a negative influence of the carboxylates on enantioselection.

Introduction

Vibrational spectroscopy, most prominently infrared spectroscopy, plays an important role in heterogeneous catalysis research for the characterization of catalyst materials, adsorbate layers, and in situ studies.[1] A vibrational spectrum contains detailed information on the nature of adsorbed molecules, their orientation with respect to the surface, and their bonding to the surface. Furthermore, the information contained in vibrational spectra is now becoming readable in more and more detail by comparison with theoretical spectra due to the advent of sophisticated density functional theory calculations and high speed computers.

In recent years, in situ spectroscopy, that is, the spectroscopy of a catalyst system at work, has been realized to be a powerful tool for fundamental catalysis research.[2] The correlation of catalytic outcome with spectroscopic features provides direct insight into the mechanism of a catalytic reaction and the nature of the active site. Vibrational spectroscopy has been widely applied to study catalytic gas−solid interfaces in situ.[1] On the other hand, catalytic solid−liquid interfaces have hardly been studied in situ by vibrational spectroscopy, nor by other techniques, despite their importance in catalysis and many other branches in modern technology. An exception to this is represented in the work in the field of electrochemistry.[3] In situ vibrational spectroscopy of catalytic solid−liquid interfaces is experimentally challenging in many respects: (1) The signals of interest from the interface are usually much smaller than the (unwanted) signals of the liquid phase, (2) sensitivity, i.e., low signal-to-noise ratio, is usually a problem, and (3) spectra may be complicated by the many species present at the interface, ranging from reactants, intermediates and products to spectators. Furthermore, the question whether an adsorbate is an intermediate or a spectator is sometimes very difficult to answer.

It is the main aim of this contribution to present a method that holds great potential for in situ vibrational spectroscopy of catalytic solid−liquid interfaces. The technique is based on attenuated total reflection (ATR) spectroscopy and the phase-sensitive detection of periodically varying signals. The main advantages of the method are the sensitivity enhancement with respect to conventional time-resolved spectra, resulting in high quality difference spectra and the possibility to disentangle crowded spectra. This makes the method especially prone for the study of catalytic solid−liquid interfaces. Furthermore, kinetic information can be extracted.

As an example, the method is applied to the enantioselective hydrogenation of a pyrone over a Pd/TiO_2 powder catalyst. In recent years, there has been considerable interest in the enantioselective hydrogenation of C=O and C=C bonds by supported Pt and Pd catalysts, respectively, chirally modified by cinchona alkaloids.[4−7] Direct spectroscopic information from the catalytic solid−liquid interface is still largely missing. Such information is especially important for unraveling the mechanism of this complex reaction. Recently, adsorption of the modifier cinchonidine has been studied in the presence of solvent and hydrogen on a Pt/Al_2O_3 model catalyst[8,9] and in the presence of a solvent on a Pt foil.[10] Here, we report in situ vibrational spectroscopic information from the solid−liquid interface of a working powder catalyst.

Modulation Excitation Spectroscopy and Phase-Sensitive Detection. If a system is disturbed by periodically varying an external parameter such as temperature, pressure, or concentration of a reactant, then all the species in the system, which are affected by this parameter will also change periodically at the

* To whom correspondence should be addressed. Phone: ++41 1 632 22 67. Fax: ++41 1 632 11 63. E-mail: buergi@tech.chem.ethz.ch.

10.1021/jp0255987 CCC: $22.00
Published on Web 09/14/2002

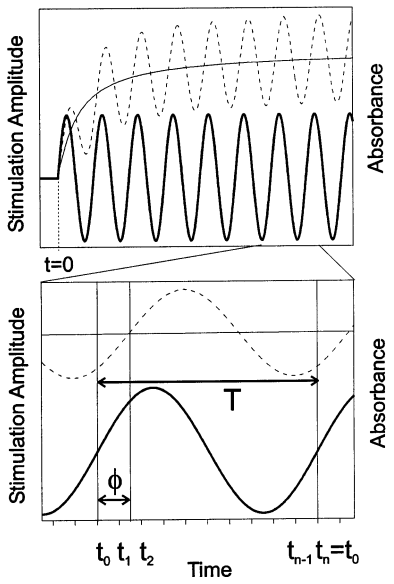

Figure 1. Schematic behavior of the absorbance of a species whose concentration in the system is affected by a periodic, in this case a sinusoidal, change of an external parameter. Thick solid line: stimulation amplitude; dashed line: absorbance $A(\tilde{\nu},t)$ of a species in the system at a certain wavelength, thin solid line: mean absorbance $A_0(\tilde{\nu})$. At $t = 0$ one parameter in the system starts to be modulated with a certain stimulation amplitude around a mean value. The concentration of species, which are affected by the external stimulation, and hence, the absorbance associated with these species, are periodically changing at the same frequency as the stimulation. After an initial period a quasi stationary state is reached at which the mean absorbance is constant. Typically modulation experiments are performed at this stationary state by recording n time-resolved spectra at t_0, t_1,...t_n, within the modulation period T. Data acquisition is synchronized with the stimulation. The response (absorbance) can be retarded with respect to the stimulation (phase lag ϕ).

same frequency as the stimulation, or harmonics thereof (Figure 1).[11] It is possible that there is a phase lag ϕ between excitation and response. This happens when the time constant of the process giving rise to some signal is on the order of the time constant $2\pi/\omega$ of the excitation. Also, the response possibly has a different shape as the excitation if the system response is nonlinear. At the beginning of the modulation, the system relaxes to a new quasi stationary state around which it is oscillating at frequency ω, as depicted in Figure 1. In this quasi stationary state the absorbance variations $A(\tilde{\nu},t)$ are followed by measuring spectra at different times t_0, t_1,...t_n within the modulation period T (Figure 1). This set of spectra, the time-resolved absorbance spectra, are then converted into phase-resolved absorbance spectra according to eq 1

$$A_k^{\phi_k^{\mathrm{PSD}}}(\tilde{\nu}) = \frac{2}{\mathrm{T}}\int_0^{\mathrm{T}} A(\tilde{\nu},t)\sin(k\omega t + \phi_k^{\mathrm{PSD}})dt$$

$$k = 1,2,.... \qquad (1)$$

Mathematically, a phase-sensitive detection (PSD) is done by multiplying $A(\tilde{\nu},t)$ by a sine function of the same frequency as the stimulation or harmonics thereof, $\sin(k\omega t+\phi_k^{\mathrm{PSD}})$, followed by a normalized integration of the product over the modulation period T. With one set of time-resolved spectra eq 1 can be evaluated for different phase settings ϕ_k^{PSD} to get different phase-resolved absorbance spectra. The variable k determines the frequency, at which the time-dependent signals are demodulated, i.e., fundamental of the excitation frequency, first harmonic, and so on. Note that the described procedure is analogous to a digital lock-in amplification. The advantages of this technique will be discussed using the example of the enantioselective hydrogenation of 4-methoxy-6-methyl-2-pyrone.

SCHEME 1: Scheme of the Reaction of 4-Methoxy-6-methyl-2-pyrone (1) to 5,6-Dihydro-4-methoxy-6-methyl-2-pyrone (2)

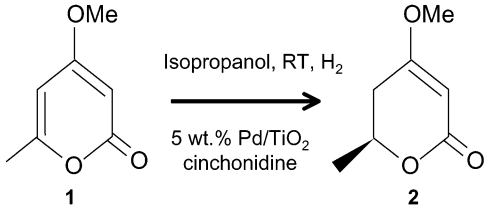

Experimental Section

Preparation of Catalyst Layer. The hydrogenation of 4-methoxy-6-methyl-2-pyrone (**1**) to 5,6-dihydro-4-methoxy-6-methyl-2-pyrone (**2**) was carried out in 2-propanol (Baker analyzed) at room temperature and one bar using a 5 wt % Pd/TiO_2 catalyst (Scheme 1). 4-methoxy-6-methyl-2-pyrone (**1**) was synthesized as described earlier [12] and purified by sublimation in a vacuum (140 °C, 0.1 mbar). The catalyst (metal dispersion 0.18, determined by H_2 chemisorption) was prepared from TiO_2 (P25, Degussa, 55 m^2/g) and $PdCl_2$ as described elsewhere and reduced in situ.[13] A slurry of 10 mg catalyst in 5 mL 2-propanol was stirred for 30 min. Then, a ZnSe internal reflection element (IRE, 45°, 50 × 20 × 2 mm, KOMLAS) was covered by dropping the slurry on its one side. The solvent was allowed to evaporate and the procedure was repeated five times. After drying 10 h, the catalyst layer was ready for use. Prepared in this way, the catalyst layer adhered to the IRE such that no loss of catalyst was observed over the course of several hours under flow through conditions (see below). The catalyst exposed to the reaction mixture, a film of 3.1 cm^2 area, amounted to 1−1.5 mg. For each experiment, a fresh catalyst layer was used.

ATR Spectroscopy and Data Acquisition. Attenuated total reflection (ATR) spectra were recorded using a home-built stainless steel flow through cell. The gap between the polished steel surface of the cell and the IRE is 250 μm and defined by a 30 × 1 mm viton O-ring (Johannsen AG) fit into a precision electro-eroded nut of the steel cell. The length and width of the exposed area of the IRE is 42.8 and 7.5 mm, respectively. The edges of the exposed area are rounded off to avoid stagnant regions of the flowing liquid. The total volume of the cell is 0.077 mL. The flow-through cell can be heated and cooled by means of a thermostat. The measurements reported here were all performed at room temperature.

After assembling, the cell was mounted onto an ATR attachment (OPTISPEC) within the Fourier transform IR spectrometer (Bruker, IFS-66/S). At the entrance and exit of the IRE the IR beam was collimated to minimize signal contributions from the O-ring region.

Liquid was flown over the sample by means of a peristaltic pump (ISMATEC Reglo 100) located after the cell. Liquid was provided from two separate glass bubble tanks, where the liquids could be saturated with gases. The flow from the two tanks was controlled by a pneumatically actuated three way Teflon valve (PARKER PV-1−2324). Teflon tubing was used throughout.

After purging the sample compartment of the spectrometer with dry air for about 1 h, neat 2-propanol saturated with hydrogen (PANGAS, 99.999%) was admitted to the sample for

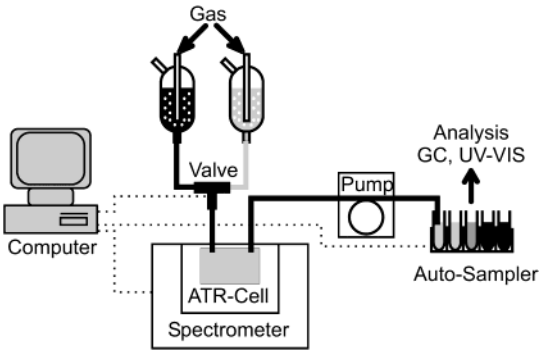

Figure 2. Schematic experimental setup. The measurement program controls the timing of the data acquisition, the valve switching and sample collection for off-line analysis (dotted lines).

10−20 min. At the end of this period, a spectrum was collected by co-adding 200 interferograms, which served as the reference for all subsequent absorption measurements. Modulation was then started by periodically varying the concentration of the reactant **1** by pumping alternatively the solutions of the two bubble tanks over the sample. Actual data acquisition was started after typically six full modulation periods. This initial time has to be allowed for the sample to reach a quasi stationary state, where the mean absorbance per period (dc term)

$$A_0(\tilde{\nu}) = \frac{1}{T}\int_0^T A(\tilde{\nu},t)dt \qquad (2)$$

is constant (Figure 1). Measurement of the time-resolved spectra was synchronized with the concentration modulation by switching the computer-controlled valve within the data acquisition loop. During one modulation period $T = 448$s, 60 spectra were measured by co-adding several interferograms per spectrum, at a speed of about eight interferograms per second and a resolution of 4 cm^{-1}. Signal averaging was performed over six modulation periods. The solution exiting the cell was collected phase-resolved using an auto-sampler, which was also synchronized with data acquisition. Typically, 10 different samples were collected within one modulation period. The collected samples were then analyzed using a HP 6890 gas chromatograph. A Chiralsil-DEX CB column (Chrompack) was used to determine the enantiomeric excess (ee). In the presence of cinchonidine the *S*-enantiomer was produced in excess.[14] A schematic of the experiment is shown in Figure 2.

Data Analysis. At the end of the data acquisition, the 60 averaged interferograms were Fourier transformed and converted into the time-resolved absorbance spectra using the spectrum recorded before starting the modulation as the reference. The time-resolved absorbance spectra were then transformed into phase-resolved absorbance spectra using eq 1. Ten phase-resolved absorbance spectra were calculated by varying the phase angle ϕ_1^{PSD} in 18° steps between 0 and 180°. Only phase-resolved absorbance spectra with frequency corresponding to the fundamental ($k = 1$) are reported here. Note that phase-resolved absorbance spectra with ϕ_1^{PSD} differing by 180° are identical but for the sign of the absorbance signals.

Results

System Characteristics. The excitation function under the same conditions as used for the experiments was measured by modulating between 2-propanol and a solution of **1** (3.6 mmol/l) in 2-propanol and following the absorbance of the strong band of **1** at 1570 cm^{-1} as a function of time. Figure 3 shows the absorbance at 1570 cm^{-1} as a function of time, as well as the first derivative thereof. The flow rate was, as in the experiments, 0.5 mL/min and time $t = 0$ s corresponds to the switching of the valve. As can be seen from Figure 3, it takes about 30 s for the solution to reach the ATR cell (corresponding to 0.25 mL volume). The measured excitation function resembles a square wave. The deviation from an ideal square wave arises for several reasons. First, the solution is spread due to some backmixing (dispersion) in the tubing between valve and cell, that is the residence time distribution in this volume deviates from a Dirac delta function. Second, the ATR cell itself has a finite volume, which takes time to be filled or exchanged from one solution to the other. From the volume of the cell (0.077 mL) and the pumping speed (0.5 mL/min), an exchange time of about nine seconds can be calculated. Finally, diffusion of the reactants through the stagnation layer in the flow-through cell has to be considered. The root-mean-square path traveled by a molecule in time t is given by $\langle x^2\rangle^{1/2}=(2Dt)^{1/2}$. Assuming a stagnation film thickness of 100 μm (conservative estimate for a total gap thickness of 250 μm) and a diffusion constant D of 10^{-5} cm^2/s a time of 5 s is needed for the molecules to reach the volume probed by ATR. The peak in the first derivative of the time dependence of the tracer signal has a full width at half-maximum of around 20 s.

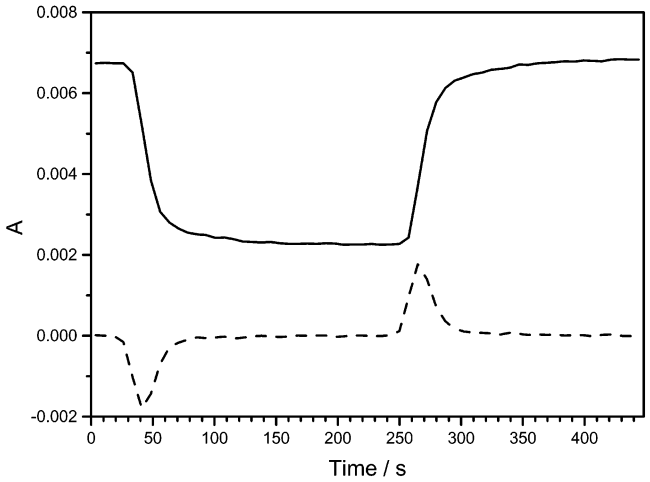

Figure 3. ATR signal of **1** at 1570 cm^{-1} as a function of time within a modulation period (full line) and first derivative thereof (dashed line). The ATR spectra were recorded over a bare ZnSe internal reflection element. The concentration of **1** was modulated between 0 and 3.6 mmol/l. Flow rate: 0.5 mL/min.

Figure 4 (top) shows a single beam ATR spectrum collected, while flowing 2-propanol over the internal reflection element covered with the catalyst. The solvent strongly absorbs the light between 1100 and 1270 cm^{-1} and between 1300 and 1480 cm^{-1}. Despite the strong absorption accurate compensation of the solvent signal can be achieved as will be obvious in the next sections, making it possible to detect signals, which are 3 to 4 orders of magnitude weaker than the ones from the solvent. Figure 4 also shows the ATR spectra of solutions of the reactant **1** and the product **2** (see Scheme 1) in 2-propanol.

Racemic Reaction. Figure 5 shows some time-resolved absorbance spectra of an experiment, where the concentration of the reactant **1** was modulated between 0 and 3.6 mmol/l at a frequency of 0.00223 Hz (modulation period $T = 448$ s). As the reference served the spectrum recorded after flowing hydrogen saturated 2-propanol over the Pd/TiO_2 catalyst for about 10 min. Several relatively strong bands (on the order of one % absorbance or more) are evident, which arise when admitting **1** to the catalyst. These bands are associated with species adsorbed on the Pd/TiO_2 catalyst and do not resemble

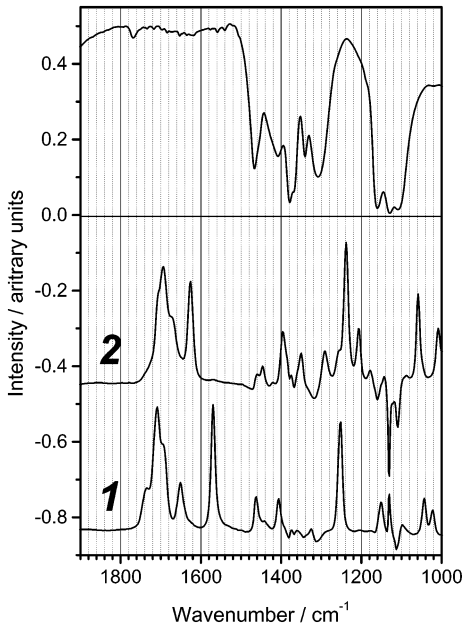

Figure 4. Top: Single beam ATR spectrum of 2-propanol over a ZnSe internal reflection element. Bottom: ATR spectra of **1** and **2** (17.6 mmol/l) in 2-propanol. Spectra are given as absorbance spectra with the neat 2-propanol as the reference. Spectra are scaled and offset.

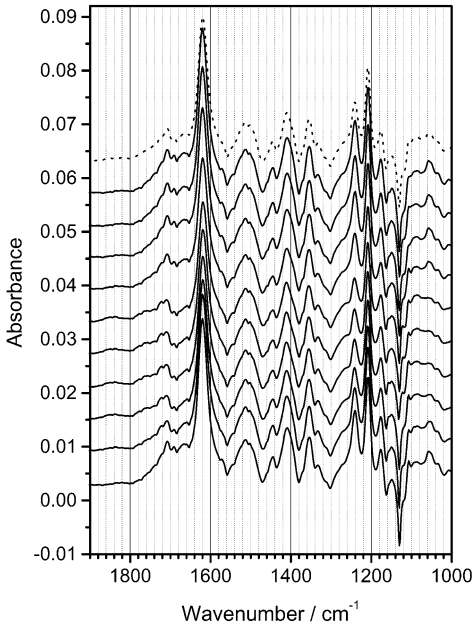

Figure 5. Time-resolved ATR spectra of a modulation experiment. The concentration of the reactant **1** was modulated between 0 and 3.6 mmol/l with a modulation period of 448s. Solvent: Hydrogen saturated 2-propanol; catalyst: 5 wt % Pd/TiO_2. The last spectrum after exposing the catalyst to hydrogen saturated 2-propanol for 10 min was used as the reference. The spectra were recorded after (from bottom to top) 3.7, 48.5, 93.3, 138.1, 182.9, 227.7, 272.5, 317.3, 362.1, and 406.9 s. The top spectrum (dotted) corresponds to the mean absorbance spectrum per period (dc term, see eq 2). No cinchonidine was used.

the spectra of neither reactant (**1**) nor product (**2**) as a comparison with Figure 4 shows. All of these time-resolved spectra strongly resemble the mean absorbance spectrum (dotted spectrum in Figure 5, eq 2), that is the spectra do not change much with time, even though the concentration of the reactant was modulated. Hence, most of the intensity observed in the spectra is static (large dc-term). Some changes are noticeable at around 1700, 1240, and at 1060 cm^{-1}. The information concerning the part of the intensity, which is periodically

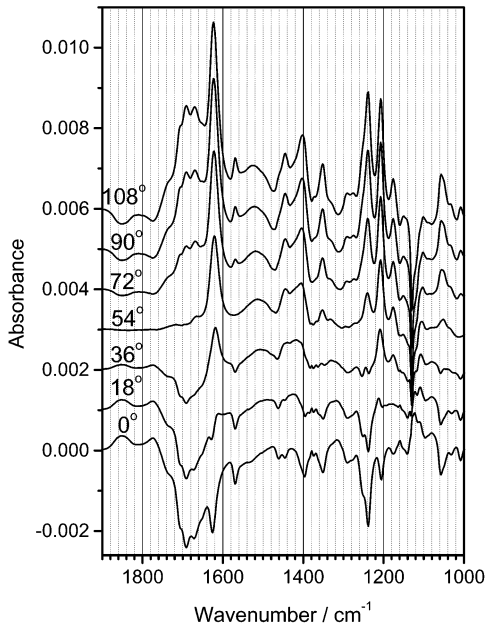

Figure 6. Phase-resolved ATR spectra obtained from the data set depicted in Figure 5 by applying the phase-sensitive detection scheme given in eq 1. Spectra were calculated for different phase-settings ϕ^{PSD} between 0 and 108°. Phase settings are given for each phase-resolved spectrum.

changing with time due to the concentration modulation, is hard to read from these spectra. Obviously, difference spectra are needed to visualize the changes.

Figure 6 shows such difference spectra, which are obtained from the data set shown in Figure 5 by applying the phase-sensitive detection scheme given in eq 1. Spectra are given for different phase-settings ϕ^{PSD} between 0° and 108°. The given phase-settings were not corrected for the time required for the solution to flow from the valve to the cell. However, absolute phase angles are not of importance here. The applied phase-sensitive detection scheme is an easy way to separate the changing (ac-term) from the static signals (dc-term). In this example, the static are more intense than the changing signals by about 1 order of magnitude. However, the changing signals are at least as important as the static ones in order to learn about the catalytic reaction.

Comparison between Figures 5 and 6 reveals quite large differences between the time- and phase-resolved spectra. This is a direct consequence of the separation of the static signals from the changing ones by the phase-sensitive detection. Also, the phase-resolved spectra strongly change with phase-setting ϕ^{PSD}. This shows that species with different kinetic response toward the modulation of the reactant concentration give rise to the overall spectrum. By choosing the phase-setting accordingly, all the signals associated with a particular species completely vanish. This is demonstrated in Figure 6 for the signals of the dissolved reactant **1**. The most prominent bands of **1** in solution are found at 1710, 1570, and 1252 cm^{-1} as shown in Figure 4. These signals vanish at a phase-setting of 54°, best seen for the band at 1570 cm^{-1}, which is not overlapping with other bands.

The phase-resolved spectra represent high quality difference spectra. For example the relatively weak and broad bands at 1850 and 1770 cm^{-1} are easily detected in the phase-resolved spectra, whereas these bands are hardly detectable in the time-resolved spectra. The noise level of the spectra determined in the spectral region between 1900 and 2000 cm^{-1} is about 1×10^{-4} absorbance units for the time-resolved and 5×10^{-6} for

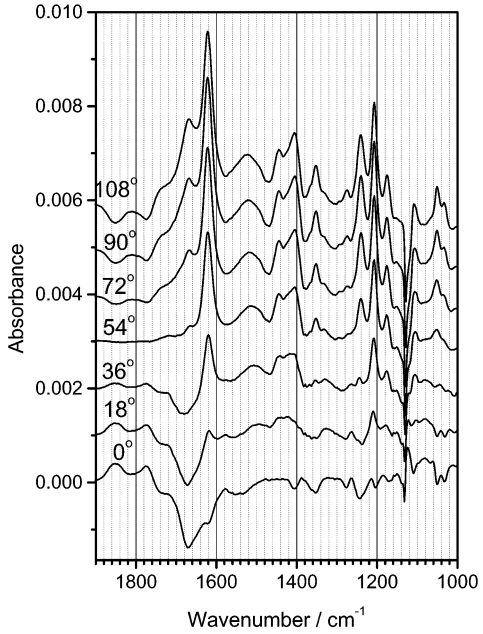

Figure 7. Phase-resolved ATR spectra. The spectra were obtained from the data set depicted in Figure 6 by subtracting the contribution of dissolved reactant (**1**) and product (**2**).

the phase-resolved spectra. The better noise-level by more than one order of magnitude is due to the fact that phase-sensitive detection is a narrow band technique, that is, noise only contributes from a frequency range close to the modulation frequency.

In a crowded spectrum, composed of bands from many species, the association of bands to the different species can be very cumbersome. Analysis of the phase-resolved spectra is very helpful in this respect. Bands belonging to the same species show identical time and phase behavior, and hence, they vanish at the same phase-setting ϕ^{PSD}. For example, the bands at 1350 and 1570 cm^{-1} in Figure 6 vanish at around 36 and 54° and can hence not belong to the same species. Furthermore, in crowded spectra overlap of bands is usually observed, which prevents exact determination of band characteristics such as positions and widths. Phase resolution of overlapping bands is another useful attribute of phase-sensitive detection. If two overlapping bands belong to species with different kinetics there is always a phase angle where one band is completely vanishing, leaving the other band undisturbed. Phase resolution is for example obvious for the two overlapping bands at 1240 and 1255 cm^{-1} in Figure 6. It can be seen in Figures 5 and 6 that the solvent is disturbing only in a very narrow spectral range at 1130 cm^{-1}. The single beam spectrum in Figure 4 shows that at this frequency about 99% of the infrared radiation is absorbed.

Many signals in the phase-resolved spectra in Figure 6 are associated with dissolved reactant and product. However, these signals can easily be eliminated, since the spectra of reactant and product can be measured independently. This was done by subtracting the ATR spectra of dissolved **1** and **2** (Figure 4) from the phase-resolved spectra shown in Figure 6. The resulting difference spectra are shown in Figure 7. It should be noted that this subtracting procedure can become complicated if several dissolved species are present. In the present case, GC analysis showed that no other products than **2** were formed in significant amount. The bands in the difference spectra shown in Figure 7 are associated with adsorbed species. The appearance of product (**2**) in both the ATR spectra and the off-line GC

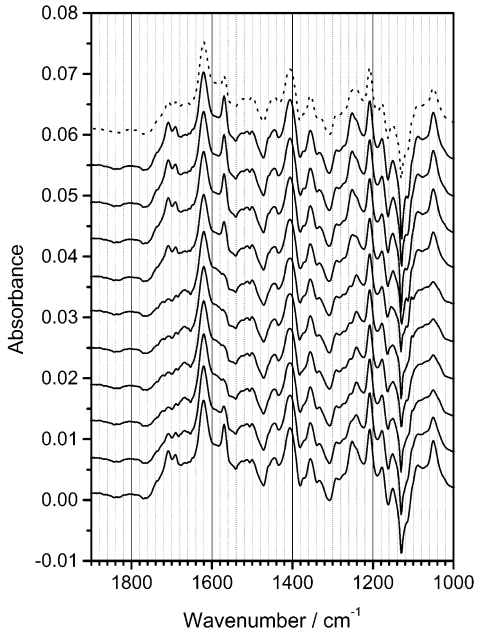

Figure 8. Time-resolved ATR spectra of a modulation experiment. The spectra were recorded after (from bottom to top) 3.7, 48.5, 93.3, 138.1, 182.9, 227.7, 272.5, 317.3, 362.1, and 406.9 s. The top spectrum (dotted) corresponds to the mean absorbance spectrum per period (dc term, see eq 2). Conditions are identical to the ones used for recording the spectra shown in Figure 5 with the exception that 2×10^{-5} mol/l cinchonidine was added to both the 2-propanol and the solution of **1**. The reference spectrum was measured in the absence of cinchonidine.

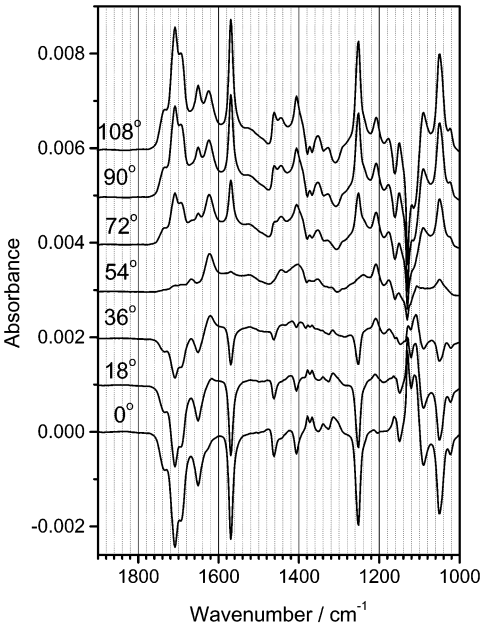

Figure 9. Phase-resolved ATR spectra obtained from the data set depicted in Figure 8 by applying the phase-sensitive detection scheme given in eq 1. Spectra were calculated for different phase-settings ϕ^{PSD} between 0 and 108°. Phase settings are given for each phase-resolved spectrum.

analysis demonstrates that the spectra were recorded truly in situ, that is, while the catalyst was working.

Enantioselective Reaction. Figures 8 and 9 show spectra of an analogous experiment as the one depicted in Figures 5 and 6 with the exception that 2×10^{-5} mol/l cinchonidine were added to both tanks (Figure 2). Apart from this slight difference all other parameters were identical for the two experiments. The results are distinctly different in several respects. In the time-

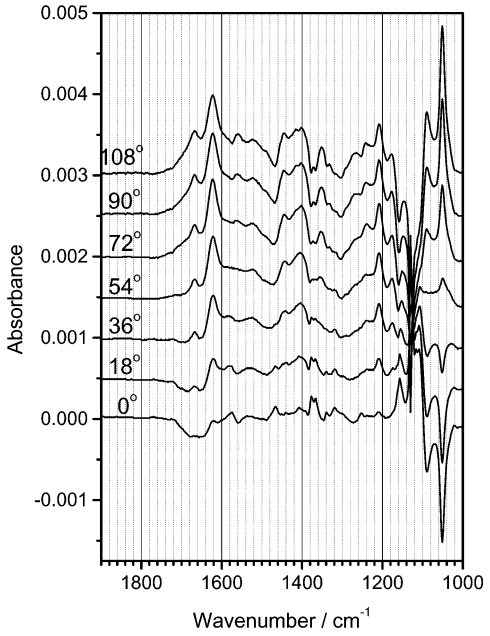

Figure 10. Phase-resolved ATR spectra. The spectra were obtained from the data set depicted in Figure 9 by subtracting the contribution of dissolved reactant (**1**) and product (**2**).

resolved spectra (Figures 5 and 8), the presence of cinchonidine leads to different relative intensities of some bands and in general to weaker bands. It should be noted that the absolute intensity (absorbance) of the bands depends on the amount of catalyst probed by the infrared radiation, which can vary from experiment to experiment. The reproducibility of the absolute intensity of the bands was however relatively good (10−15%). The effect of cinchonidine in reducing the signal intensities in the time-resolved spectra was confirmed by performing an experiment without cinchonidine and subsequently one in the presence of cinchonidine on the same catalyst layer.

Addition of cinchonidine also has a large effect on the phase-resolved spectra. (Figures 6 and 9). In the presence of (a minute amount of) cinchonidine, the most prominent features can be assigned to the reactant in solution, whereas in the absence of cinchonidine the reactant signals are relatively small. This is best seen for the sharp band at 1570 cm^{-1}, which has an absorbance of 0.0004 in the spectrum at a phase setting of 0° for the racemic reaction (without cinchonidine) and 0.0023 for the reaction in the presence of cinchonidine. This is a direct consequence of the different apparent hydrogenation rates in the presence and absence of the cinchonidine modifier. From the GC analysis of the reaction products collected at the outlet of the flow-through cell, a rate deceleration by a factor of about seven due to the presence of 2×10^{-5} mol/l cinchonidine was found. In the racemic (enantioselective) reaction, an overall conversion of 15% (2%) was determined by GC analysis for steady-state operation, i.e., for continuous flow of the reactant solution. Rate deceleration in the presence of modifier was also observed for the same reaction in a batch reactor.[14] The rate deceleration depends on the concentration of cinchonidine. At higher modifier concentrations (4×10^{-4} mol/l) the rate drastically dropped.

Again, the ATR spectra of the reactant (**1**) and product (**2**) were subtracted from the phase-resolved spectra shown in Figure 9. The resulting difference spectra are given in Figure 10.

An interesting difference between the reaction in the presence and absence of cinchonidine is the behavior of the broad bands at 1770 and 1850 cm^{-1}. In the phase-resolved spectra, these bands are clearly visible for the experiment performed in the absence of cinchonidine but absent in the presence of cinchonidine. In the absence of cinchonidine the abundance of the species associated with these bands is anti-correlated to the abundance of the reactant. As can be seen in Figure 6, the signals at 1770 and 1850 cm^{-1} are positive, when the reactant signals are negative and vice versa. Also, both the 1770 and 1850 cm^{-1} signals and those of the reactant **1** vanish at the same phase-setting of 54° (or 234°). On the other hand, negative signals at 1770 and 1850 cm^{-1} are clearly seen in the time-resolved spectra in Figure 8 for the experiment in the presence of cinchonidine. Note that the reference spectrum was taken in the absence of cinchonidine before starting the modulation. This means that upon addition of cinchonidine the species associated with the 1770 and 1850 cm^{-1} bands are at least partly removed from the surface.

Apart from the obvious drastic effect induced by the minute amount of cinchonidine added to the feed, as just described, there are no spectroscopic features apparent in Figures 8 and 9, which could be assigned to cinchonidine. On the basis of a detailed investigation of cinchonidine on Pt/Al_2O_3[8,9] and Pd/Al_2O_3[15] model catalysts, we would expect bands at around 1510 and 1590 cm^{-1} for weakly N-lone pair bonded cinchonidine, at around 1530 cm^{-1} for α-H abstracted cinchonidine and at 1570 cm^{-1} for cinchonidine with the quinoline ring preferentially parallel to the metal surface. Whereas the α-H abstracted cinchonidine is not expected in large amounts on Pd[15] the most prominent band of the flat adsorbed cinchonidine is covered by the strong reactant band at 1570 cm^{-1}. The absorbance that can be expected for the cinchonidine bands can be estimated by a comparison between the signals of saturated CO and cinchonidine layers on a model catalyst and a CO layer on the Pd/TiO_2 catalyst. Such an estimate showed that the cinchonidine signals may be hard to be detected in the time-resolved spectra, but should be well above the noise level in the phase-resolved spectra. Their absence therefore indicates that with the reactant modulation the cinchonidine signals are not much altered.

Time Dependence of ATR Signals and Enantiomeric Excess (ee). Figure 11 shows the time dependence of some infrared bands for the experiment performed in the presence of cinchonidine (Figure 8). Trace *a* corresponds to the reactant, trace *b* to the product and traces *c* and *d* to species absorbing at 1680 and 1620 cm^{-1}, respectively. Figure 11 demonstrates the feasibility to directly correlate time-dependent spectroscopic signals with reaction behavior (here enantiomeric excess) for catalytic reactions at solid−liquid interfaces. Clearly, the reactant, the product, and the species associated with the band at 1680 cm^{-1} show very similar time dependence. This is then also reflected in the similar phase-setting in the phase-resolved spectra (Figures 9 and 10, Table 1) at which the corresponding bands vanish. In contrast, the species associated with the band at 1620 cm^{-1} exhibits distinctly different time behavior, also reflected in the phase lag of about 50° with respect to the reactant (Figure 9).

The kinetics of a species, and hence also the phase-lag, may be very helpful for the decision whether a species is a spectator or possibly involved in the catalytic cycle. In our example, and on the time-scale of the experiment, the reactant and product indicate similar time behavior as shown in Figure 11. The species associated with the band at 1680 cm^{-1} also shows similar time-dependence. Hence, this species *could* be involved in the catalytic cycle. On the other hand, the species associated with the band at 1620 cm^{-1} shows distinctly different kinetics and thus exhibits a phase-lag with respect to the reactant. This

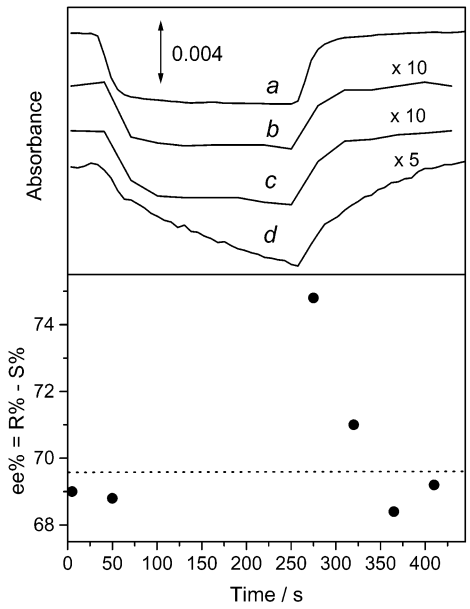

Figure 11. Time dependence of (top) the intensity of various bands depicted in Figure 8 and (bottom) enantiomeric excess (ee) within one modulation period. The time required for the solution to flow from the cell to the auto-sampler was accounted for in order to compare corresponding spectroscopic signals and enantiomeric excess. Top: (a) absorbance of the band at 1570 cm^{-1} (reactant, **1**), (b) absorbance of the band at 1692 cm^{-1} (product, **2**), (c) absorbance of band at 1680 cm^{-1}, (d) absorbance of band at 1620 cm^{-1}. Traces a and d were directly determined from the time-resolved spectra (Figure 8). Traces b and c were determined by first subtracting the contributions of the dissolved reactant from the time-resolved spectra. Note that traces a and d were constructed from 60 points (according to 60 time-resolved spectra), whereas traces b and c from 15 points only. Dotted line: Steady-state value of ee measured for continuous flow.

species can be excluded as an intermediate in the transformation of **1** to **2**. However, it should be noted that a species, which is not an intermediate can still influence the outcome of a reaction, for example through adsorbate−adsorbate interaction. Such complex behavior is indeed indicated by the comparison of the time-dependence of the spectroscopic signals and the measured enantiomeric excess (ee) in Figure 11. As is obvious, the ee is not constant during the modulation period. When the reaction is turned on by admitting the reactant the ee is initially close to 75% but decreases afterward to about 69%, which is close to the steady-state value of 69.6% (dotted line in Figure 11). Even though the time-resolution of the measured ee is not very high, the decay in ee is slower than the increase of the signals associated with the reactant and product. The measured ee rather follows the appearance of the signal at 1620 cm^{-1}, which may indicate that the presence of the species associated with the band at 1620 cm^{-1} has a (slight) negative influence on enantiodifferentiation.

Discussion

Concentration Modulation Excitation Spectroscopy and Phase-Sensitive Detection. As demonstrated in the results section, major advantages of the method are: (i) With respect to conventional difference spectra at least one order of magnitude better signal-to-noise can be obtained. This is mainly due to the fact that phase-sensitive detection is a narrow-band technique. Furthermore, signal-to-noise can be improved by averaging over several modulation periods, without losing time-(phase-)resolution. This point is very important for investigations at catalytic solid−liquid interfaces, where the signals from the adsorbed species are typically small. (ii) Phase-sensitive detection allows the unambiguous separation of static (dc-term) and periodically varying (ac-term) signals. (iii) Direct kinetic information can be gained. Species, which show different characteristic time constants for the processes induced by the excitation, will exhibit different phase-lags. This phase-lag and the modulation amplitude of a signal can be rigorously correlated to the underlying kinetics, which has not been demonstrated here.[16−18] The phase lag between excitation and response and the modulation amplitude of a signal associated with a certain species depend on the modulation frequency. This gives the operator an additional degree of freedom. However, it should be noted that rigorous kinetic treatment can become quite tedious for complicated kinetics. For quantitative kinetic treatment a sinusoidal excitation function largely simplifies the analysis. (iv) Crowded spectra, which are usually encountered for catalytic solid−liquid interfaces can easier be analyzed, if species exhibit different phase lags. This allows for the unambiguous subtraction of the bands associated with one species by choosing the appropriate phase-setting. Also, slowly responding species can be suppressed in the spectra by increasing the modulation frequency. (v) Phase resolution of overlapping bands can be achieved for bands with different phase lag. A limitation is the fact that only processes that are reversible, at least to a certain degree, can be investigated using phase-sensitive detection.

The time resolution of the method is limited by several factors. One factor is the time resolution of the spectrometer. For concentration modulation excitation of heterogeneous reactions at the solid−liquid interface, this is usually not the limiting factor. Modern FTIR spectrometers allow one to record on the order of 100 spectra/s. For concentration modulation experiments, external and pore diffusion phenomena may disguise the intrinsic kinetics of the reaction occurring at the catalytic solid−liquid interface. External diffusion of the reactants or products through the stagnation layer in the flow-through cell takes on the order of a second. Another limiting factor is the time needed to fill the cell, which was about nine seconds for the applied conditions. This time can be considerably reduced, by increasing the throughput or decreasing the cell volume. Finally, the flow behavior of the liquid within the volume before the cell represents another limiting factor.

It should be emphasized that the modulation excitation and phase-sensitive detection is limited neither to concentration modulation nor ATR infrared spectroscopy. Parameters that can be modulated are, besides concentration, pH, temperature, pressure, photon flux (in a photocatalytic reaction) and electric field for example. The method can be applied to any spectroscopic technique where time-resolved spectra can be recorded, such as UV−vis, Raman, IRRAS (infrared reflection absorption spectroscopy), DRIFTS (diffuse reflection infrared Fourier transform spectroscopy), and XANES (X-ray absorption near edge spectroscopy), just to mention a few.

Finally, it should be noted that modulation spectroscopy and phase-sensitive detection as presented above can be viewed as a statistical analysis of time-resolved spectra highlighting the correlation of spectroscopic signals. As such, it is conceptually similar to the 2D-IR spectroscopy introduced by Noda.[19]

Assignment of Bands. The bands observed in the spectra and their assignment is summarized in Table 1. The most prominent feature in the time-resolved spectrum in the absence of cinchonidine shown in Figure 5 is the band at 1620 cm^{-1}. Note that the reference for these spectra was taken before the concentration modulation, i.e., in the absence of **1**. Hence, the

TABLE 1: Observed Vibrational Bands in the Time- and Phase-Resolved Spectra Depicted in Figures 5−10 for the Concentration Modulation Excitation Experiments in the Presence and Absence of Cinchonidine

without modifier		with modifier		
time-resolved	phase-resolved	time-resolved	phase-resolved	assignment
	1850 (234)	1840		CO; ν(CO)
	1770 (234)	1760		CO, HCO; ν(CO)
		1720	1736 (54)	**1**; ν(C═O)
1710	1710 (54)		1710 (54)	**1**, **2**; ν(C═O)
	1692 (54)		1692 (54)	**1**; ν(C═O)
	1680 (50)[a]		1670 (50)[a]	ν(C═O)
	1670 (36)	1670	1670 (0)	ν(C═O)
			1650 (54)	**1**; ν(C═C)
1620	1620 (5)	1620	1620 (−5)	Carboxylate; ν_{as}(COO)
	1570 (54)		1570 (54)	**1**; ν(C═C)
1510	1520 (0)[a]	1510	1520 (0)[a]	Carboxylate; ν_{as}(COO)
	1462 (54)		1462 (54)	**1**; $\delta_a(CH_3)$
1445	1445 (0)	1445	1445 (0)	Carboxylate; $\delta_a(CH_3)$
			1408 (54)	**1**
1410[a]	1405 (5)	1410[a]	1400 (−5)	Carboxylate; ν_s(COO)
	1397 (54)			**2**
1355	1352 (24)	1355	1352 (24)	
1332		1332		
	1255 (54)		1253 (54)	**1**; δ(CH), ν(C−O)
1240	1240 (18)	1240	1240 (18)	
1210	1210 (−5)	1210	1210 (−5)	Carboxylate;δ(CH), ν(C−O)
1175	1175 (0)	1175	1175 (0)	
	1060 (54)			**2**
1060	1058 (46)	1050	1050 (46)	
	1010 (54)			**2**

Frequencies are in cm^{-1}. The number in parentheses indicates the phase-setting, at which the corresponding band vanishes. [a] Broad band.

signals in Figure 5 arise due to the admittance of **1** to the catalyst. The 1620 cm^{-1} band is also the most prominent signal in the presence of cinchonidine (Figure 8) but considerably less dominant. Furthermore, the band is visible in the phase-resolved spectra both in the presence and absence of cinchonidine (Figures 9 and 6) although considerably less intense in the former case. Analysis of the phase-resolved spectra shows that the band at 1620 cm^{-1} is correlated with a signal slightly above 1400 cm^{-1}. In the presence of cinchonidine, both the band at 1620 and the one slightly above 1400 cm^{-1} show a small phase-lag (about 10°) with respect to the experiment in the absence of cinchonidine, indicating slower kinetics of the corresponding species in the presence of cinchonidine. The band slightly above 1400 cm^{-1} is also visible in the time-resolved spectra both in the presence and absence of cinchonidine. It will be shown later that the two bands are associated with a species adsorbed on the TiO_2 support rather than on the Pd. To check whether these bands originate from the adsorption of reactant (**1**) or product (**2**) on the support, modulation experiments were performed with both the reactant and the product on the bare TiO_2 (P25) support, which clearly show that this is not the case. Figure 12 shows the phase-resolved spectrum at a phase-setting of 108° for these experiments. In both cases, the phase-resolved spectrum is very similar to the spectra of the corresponding dissolved compounds (see Figure 4). In particular, the strong band at 1620 cm^{-1} observed in the spectra in Figures 6 and 9 is missing.

Bands at 1620 and 1400 cm^{-1} are a sign for carboxylate groups on TiO_2.[20] The band at 1620 cm^{-1} can be attributed to the antisymmetric COO stretch of a bidentate carboxylate coordinated to two titanium ions, whereas the band at around 1400 cm^{-1} is assigned to the symmetric COO stretch.[20] The assignment of these bands to carboxylates is supported by the presence of the broad band at around 1510 cm^{-1}, which can be assigned to the antisymmetric COO vibration of a carboxylate chelating to a single titanium ion.[21] This band shows a similar phase-lag as the signals associated with bidentate carboxylates (Table 1).

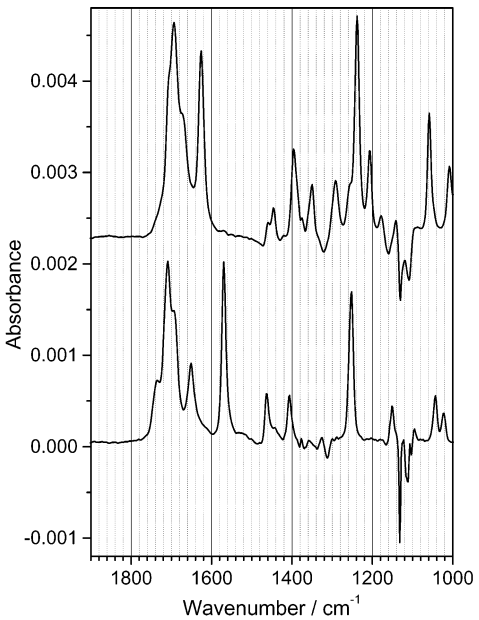

Figure 12. Phase-resolved spectra (at a phase-setting of 108°) of concentration modulation experiments. Experimental conditions were similar to the ones for the experiments shown in Figures 6 and 9. The concentration of **1** (bottom) and **2** (top) was modulated between 0 and 3.6 mmol/l, $T = 448$s, catalyst: TiO_2 (P25), solvent: hydrogen saturated 2-propanol. The negative peaks at around 1130 cm^{-1} are due to incomplete compensation of solvent signals.

The band at 1210 cm^{-1}, which is consistent with a C−H bending coupled with a C−O stretching mode, shows the same phase lag as the 1620 and 1400 cm^{-1} bands. This indicates that the adsorbed carboxylates are formed from **1**. The very intense bands of **2** at 1240 and of **1** at 1255 cm^{-1} (Figure 4) are associated with coupled C−H bending and C−O stretching modes, as a vibrational analysis at the density functional theory level shows. [22] Furthermore, a band at 1445 cm^{-1} may, based

on the similar phase-lag, correspond to the carboxylates. The corresponding band of **1** at 1462 cm^{-1} is associated with an antisymmetric CH_3 deformation mode.

In the region around 1670 cm^{-1}, at least two bands can be distinguished. A broad band, with very similar phase lag and time behavior (see Figure 11) as reactant and product, is overlapped by a sharper band at 1670 cm^{-1}. The latter band exhibits some larger phase lag with respect to the reactant. The phase lag of this band is considerably larger in the presence of cinchonidine. The observed bands at 1670 cm^{-1} may be assigned to a carbonyl coordinated to a Ti^{4+} Lewis site via the C═O oxygen[23] or an unidentate coordination of a carboxylate group.[20] Alternatively the broad band could be associated with the carbonyl group of **1** adsorbed on the Pd in a η_1 (end on) configuration.[24] This would be consistent with the similar time behavior of this species and the reactant **1** and the smaller intensity of this band in the presence of cinchonidine because adsorbed cinchonidine blocks a large fraction of the metal surface. The fact that the band was not observed on TiO_2 (P25) is also in favor of a species adsorbed on Pd.

The two bands at 1850 and 1770 cm^{-1} appear negative, when cinchonidine is added (see Figure 8), which indicates that cinchonidine competes with the species associated with these bands for adsorption sites. On the other hand, these bands arise in the phase-resolved spectra in the absence (but not in the presence) of cinchonidine exactly 180° out-of-phase with respect to the reactant. This may indicate that this species and the reactant compete for adsorption sites or hydrogen. The frequency of the band at 1850 cm^{-1} is very high for a carbonyl vibration but rather low for a CO adsorbed on Pd.[25] Similar bands at about 1831 and 1734 cm^{-1} were observed when exposing formic acid to Pd/TiO_2 in a vacuum.[26] Although no definite proof could be provided, the bands were assigned to CO and HCO at the perimeter of Pd particles. It should be noted that no significant amount of "normal" CO on the Pd particles, absorbing at 1980 cm^{-1} and above,[25] was detected on the catalyst.

Implication for the Mechanism of Enantioselective Hydrogenation. The observation of acid groups on the catalyst surface is a significant one in view of the proposed importance of acids in the mechanism of enantio-differentiation.[27−30] It has been shown lately that acids form specific interaction complexes with the modifier cinchonidine.[30] The formation of such complexes can have a pronounced effect on enantio-differentiation. Our present results show that acids can be present on the catalyst surface, even when no acids have been added to the reaction mixture.

The acids are generated when **1** is contacted with the catalyst in the presence of hydrogen. The acids are most abundant in the racemic reaction (without addition of cinchonidine), less abundant in the enantioselective reaction and not (or not to a significant amount) observed in the absence of the Pd metal. Although the chemoselectivity for the hydrogenation of **1** over the modified Pd/TiO_2 catalyst is very high,[14] our results suggest that on the catalyst surface acids are present in significant quantity. For the homogeneous asymmetric hydrogenation of 2-pyrones using a Ru catalyst in 2-propanol, alcoholysis of the lactone was observed. [31] The lactone, which is formed by hydrogenation of the C═C double bond of **2**, is easier alcoholysed (or hydrolyzed) than **1** or **2**. To confirm that it is alcoholysis (or hydrolysis) of the lactone, which leads to the observed carboxylates on the catalyst surface we synthesized the lactone. A solution of the lactone in 2-propanol was then admitted to the catalyst and independently to the P25 support. The results of these experiments are shown in Figure 13, spectra

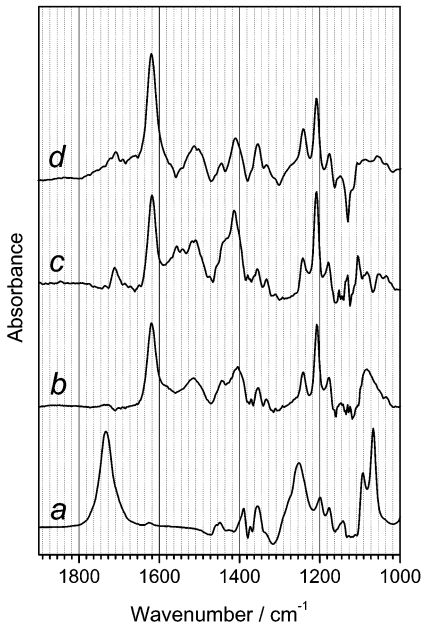

Figure 13. ATR spectra: (a) of lactone (**3**) dissolved in 2-propanol (0.001 M), (b) of the Pd/TiO_2 catalyst which was exposed to a solution of lactone (**3**) in 2-propanol and (c) of the TiO_2 (P25) support which was exposed to a solution of lactone (**3**) in 2-propanol. Spectra (b) and (c) were recorded in the presence of neat solvent. Spectrum (d) for comparison shows the mean absorbance spectrum of the modulation experiment in Figure 5.

SCHEME 2: Reactions Observed by in Situ ATR Spectroscopy

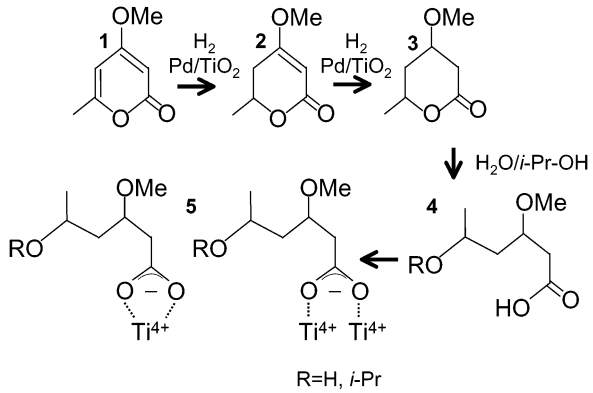

b and c. Figure 13a shows the ATR spectrum of dissolved lactone and Figure 13d shows the mean absorbance spectrum of the modulation experiment depicted in Figure 5. The large similarity of spectra b, c, and d is obvious, and demonstrates that the adsorbed carboxylates stem from the lactone. The experiments also support the assignment given in Table 1. Addition of a small amount of water did not significantly increase the amount of observed carboxylate species, which may indicate that the lactone is transformed to the acid through alcoholysis rather than hydrolysis. Scheme 2 summarizes the reactions that we observe using in situ ATR spectroscopy. In contrast to the first hydrogenation step, the lactone **3** is formed slowly. The alcoholyzed product **4** is adsorbing on the TiO_2 support in different modes. The modulation experiments show, that the carboxylates also desorb from the support, which was also confirmed by admitting lactone **3** directly to P25, followed by admitting neat solvent.

Finally, Figure 11 indicates that the presence of the acid on the catalyst surface has a negative effect on enantio-differentiation of 4-methoxy-6-methyl-2-pyrone. This is in good agreement

with catalytic experiments performed in a batch reactor, which show that acetic acid is a bad solvent.[14] One feasible explanation for this observation is that the acid competes with the reactant for the interaction with the cinchonidine.

Conclusions

Modulation excitation spectroscopy and phase-sensitive detection in combination with attenuated total reflection (ATR) infrared spectroscopy is applied to study catalytic solid−liquid interfaces of powder catalysts in situ. With respect to conventional (ATR) infrared spectroscopy, the signal-to-noise ratio can be improved by at least one order of magnitude without loosing time (phase-) resolution. The phase-sensitive detection scheme allows the separation of small varying signals from the large static ones. Analysis of the phase-resolved spectra largely helps to disentangle crowded spectra. The spectrum of a species exhibiting distinct kinetics can be unequivocally subtracted by choosing the appropriate phase-setting. Moreover, rigorous kinetic data can be gained from the analysis. The time-resolution for concentration modulation excitation spectroscopy at the solid−liquid interface is largely restricted by mass-transport. Modulation excitation spectroscopy and phase-sensitive detection is neither restricted to the modulation of reactant concentrations nor to infrared spectroscopy.

Modulation excitation infrared spectroscopy was applied to investigate the enantioselective hydrogenation of 4-methoxy-6-methyl-2-pyrone **1** over a 5 wt % Pd/TiO_2 catalyst modified by cinchonidine. Carboxylates are detected on the catalyst surface originating from alcoholysis of the lactone **3**. These carboxylates exhibit different adsorption modes (bidentate carboxylate, carboxylate chelating to a single titanium ion). The kinetics of formation and disappearance of the carboxylates from the surface is slower than the appearance and disappearance of reactant and product, resulting in a distinct phase-lag. Carbonyl vibrations are also detected. The species associated with these vibrations vary at approximately the same rate as the reactant, to within the current time resolution, and could be associated with adsorbed intermediates in the hydrogenation reaction. Furthermore, in the racemic reaction, anti-correlated to the reactant, signals appear, which are possibly associated with CO and HCO at the perimeter of the Pd particles. Cinchonidine, even at very low concentration, strongly competes with these species for adsorption sites.

In the course of the modulation period, the enantiomeric excess is not constant but is high just after the reaction is turned on and decreases within about 80 s to close to the steady-state value. The similar time-dependence of the abundance of the carboxylates and the enantiomeric excess indicates a negative influence of the carboxylates (or the acids) on the enantiodifferentiation.

Acknowledgment. We thank Dr. W.-R. Huck for the synthesis of **1** and **3** and Prof. U. P. Fringeli and Dr. D. Baurecht for discussion. Financial support from the Swiss National Science Foundation and ETH-Zürich is kindly acknowledged.

References and Notes

(1) Ryczkowski, J. *Catal. Today* **2001**, *68*, 263.
(2) Jacobs, P. W.; Somorjai, G. A. *J. Mol. Catal. A* **1998**, *131*, 5.
(3) Bockris, J. O. M.; Kahn, S. U. M. *Surface Electrochemistry: A Molecular Level Approach*; Plenum: New York, 1993.
(4) Orito, Y.; Imai, S.; Niwa, S. *J. Chem. Soc. Jpn.* **1979**, 1118.
(5) Blaser, H. U.; Jalett, H. P.; Müller, M.; Studer, M. *Catal. Today* **1997**, *37*, 441.
(6) Baiker, A. *J. Mol. Catal. A: Chem.* **1997**, *115*, 473.
(7) Baiker, A. *J. Mol. Catal. A: Chem.* **2000**, *163*, 205.
(8) Ferri, D.; Bürgi, T.; Baiker, A. *J. Chem. Soc. Chem. Commun.* **2001**, 1172.
(9) Ferri, D.; Bürgi, T. *J. Am. Chem. Soc.* **2001**, *123*, 12 074.
(10) Kubota, J.; Zaera, F. *J. Am. Chem. Soc.* **2001**, *123*, 11 115.
(11) Baurecht, D.; Fringeli, U. P. *Rev. Sci. Instr.* **2001**, *72*, 3782.
(12) De March, P.; Morena-Mañas, M.; Pi, R.; Ripoll, I.; Sánchez-Ferrando, F. *J. Heterocyclic Chem.* **1985**, *22*, 1537.
(13) Huck, W.-R.; Bürgi, T.; Mallat, T.; Baiker, A. *J. Catal.* **2001**, *200*, 171.
(14) Huck, W.-R.; Mallat, T.; Baiker, T. *Catal. Lett.* **2001**, *80*, 87.
(15) Ferri, D.; Bürgi, T.; Baiker, A. *J. Catal.* **2002**, *210*, 160.
(16) Fringeli, U. P.; Baurecht, D.; Siam, M.; Reiter, G.; Schwarzott, M.; Bürgi, T.; Brüesch, P. ATR Spectroscopy of Thin Films. In *Handbook of Thin Film Materials*; Nalwa, H. S., Ed.; Academic Press: New York, 2001; Vol. 2; p 191.
(17) Fringeli, U. P.; Baurecht, D.; Günthard, H. H. Infrared and Raman Spectroscopy of Biological Materials. In *Infrared and Raman Spectroscopy of Biological Materials*; Gremlich, H. U., Yan, B., Eds.; Dekker: New York/Basel, 2000; p 143.
(18) Ortelli, E. E.; Wokaun, A. *Vib. Spectrosc.* **1999**, *19*, 451.
(19) Noda, I. *Appl. Spectrosc.* **1990**, *44*.
(20) Roddick-Lanzilotta, A.; McQuillan, A. J. *J. Colloid Interface Sci.* **2000**, *227*, 48.
(21) Mehrotra, R. C.; Bohra, R. *Metal Carboxylates*; Academic Press: New York, 1983.
(22) Bürgi, T.; Baiker, A., unpublished results.
(23) Thistlethwaite, P. J.; Hook, M. S. *Langmuir* **2000**, *16*, 4993.
(24) Anton, A. B.; Avery, N. R.; Toby, B. H.; Weinberg, W. H. *J. Am. Chem. Soc.* **1986**, *108*, 684.
(25) Gelin, P.; Siedle, A. R.; Yates, J. T. *J. Phys. Chem.* **1984**, *88*, 2978.
(26) Chang, Z.; Thornton, G. *Surf. Sci.* **2000**, *459*, 303.
(27) Nitta, Y.; Shibata, A. *Chem. Lett.* **1998**, *161*, 161.
(28) Huck, W.-R.; Bürgi, T.; Mallat, T.; Baiker, A. *J. Catal.* **2002**, *205*, 213.
(29) Borszeky, K.; Bürgi, T.; Zhaohui, Z.; Mallat, T.; Baiker, A. *J. Catal.* **1999**, *187*, 160.
(30) Ferri, D.; Bürgi, T.; Baiker, A. *J. Chem. Soc., Perkin Trans. 2* **1999**, 1305.
(31) Fehr, M. J.; Consiglio, G.; Scalone, M.; Schmid, R. *J. Org. Chem.* **1999**, *64*, 5768.